Environmental Science & Technology

Article

Cite This: Environ. Sci. Technol. 2019, 53, 3048−3057

pubs.acs.org/est

High-Resolution Data Sets Unravel the Effects of Sources and Meteorological Conditions on Nitrate and Its Gas-Particle Partitioning

Xurong Shi,[†] Athanasios Nenes,[‡,§,∥] Zhimei Xiao,[⊥] Shaojie Song,[#] Haofei Yu,[▽] Guoliang Shi,[*,†] Qianyu Zhao,[†] Kui Chen,[⊥] Yinchang Feng,[†] and Armistead G. Russell[○]

[†]State Environmental Protection Key Laboratory of Urban Ambient Air Particulate Matter Pollution Prevention and Control, College of Environmental Science and Engineering, Nankai University, Tianjin, 300071, China

[‡]Laboratory of Atmospheric Processes and their Impacts, School of Architecture, Civil and Environmental Engineering, École Polytechnique Fédérale de Lausanne, Lausanne, CH-1015, Switzerland

[§]Institute of Chemical Engineering Sciences, Foundation for Research and Technology Hellas, Patras, Greece, GR-26504

[∥]Institute for Environmental Research and Sustainable Development, National Observatory of Athens, Palea Penteli, Greece GR-15236

[⊥]Tianjin Eco-Environmental Monitoring Center, Tianjin, 300191, China

[#]School of Engineering and Applied Sciences, Harvard University, Cambridge, Massachusetts 02138, United States

[▽]Department of Civil, Environmental and Construction Engineering, University of Central Florida, Orlando, Florida 32816, United States

[○]School of Civil and Environmental Engineering, Georgia Institute of Technology, Atlanta, Georgia 30332-0512, United States

Supporting Information

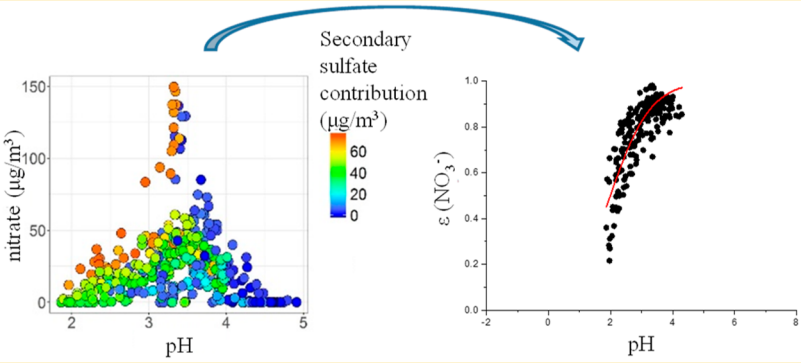

ABSTRACT: Nitrate is one of the most abundant inorganic water-soluble ions in fine particulate matter ($PM_{2.5}$). However, the formation mechanism of nitrate in the ambient atmosphere, especially the impacts of its semivolatility and the various existing forms of nitrogen, remain under-investigated. In this study, hourly ambient observations of speciated $PM_{2.5}$ components (NO_3^-, SO_4^{2-}, etc.) were collected in Tianjin, China. Source contributions were analyzed by PMF/ME2 (Positive Matrix Factorization using the Multilinear Engine 2) program, and pH were estimated by ISORROPIA-II, to investigate the relationship between pH and nitrate. Five sources (factors) were resolved: secondary sulfate (SS), secondary nitrate (SN), dust, vehicle and coal combustion. SN and pH showed a triangle-shaped relationship. When SS was high, the fraction of nitrate partitioning into the aerosol phase exhibits a characteristic "S-curve" relationship with pH for different seasons. An index (I_{TL}) is developed and combined with pH to explore the sensitive regions of "S-curve". Controlling the emissions of anions (SO_4^{2-}, Cl^-), cations (Ca^{2+}, Mg^{2+}, etc.) and gases (NO_x, NH_3, SO_2, etc.) will change pH, potentially reducing or increasing SN. The findings of this work provide an effective approach for exploring the formation mechanisms of nitrate under different influencing factors (sources, pH, and I_{RL}).

INTRODUCTION

Nitrate is a dominant inorganic component of $PM_{2.5}$ during intense haze periods in China,[1−4] and arises from secondary formation.[5,6] Nitrate is known to form through different chemical pathways during daytime and nighttime:[7−9] NO_2

Received: November 19, 2018
Revised: February 21, 2019
Accepted: February 22, 2019
Published: February 22, 2019

DOI: 10.1021/acs.est.8b06524
Environ. Sci. Technol. 2019, 53, 3048−3057

homogeneously reacting with OH radical is the most important HNO_3 formation pathway during daytime; heterogeneous hydrolysis of NO_3 and N_2O_5 is the most significant pathway of particulate nitrate during nighttime (eqs S1−S6 of the Supporting Information (SI)). Owing to its extremely low volatility, acidic H_2SO_4 resides in aerosol and tends to associate with NH_3/NH_4^+ from gas-phase to form secondary ammonium sulfate/bisulfate. When sufficient amounts of ammonia are present, HNO_3 can react with NH_3 to form ammonium nitrate.[10,11]

Nitrate concentrations in particulate matter (PM) are influenced by meteorological conditions (temperature (T), relative humidity (RH)), precursor source emissions (i.e., NO_x), the presence of other ionic species and complex gas and condensed phase chemical reactions. When relative humidity is very low, aerosol nitrate tends to be in the form of solid NH_4NO_3 according to the reaction $NH_4NO_3(s) \leftrightarrow HNO_3(g) + NH_3(g)$. Increases in temperature shifts the equilibrium to the right-hand side, meaning that nitrate remains in the gas-phase and particulate nitrate concentration is low.[12] When an aqueous phase exists in the aerosol (promoted by higher RH and lower T), it tends to completely dissolve inorganic nitrate; the volatility of nitrate then becomes strongly influenced by the acidity, or pH, of the aerosol aqueous phase.[12−17] Aerosol acidity is not only important for aerosol nitrate, but also drives the gas-particle partitioning of other acidic/basic semivolatile species.[15−17] Acidity can also play an important role in the formation of secondary organic aerosols,[13,14] and the solubility of trace nutrients that drives the toxicity and nutrient availability in atmospheric aerosol.[18−21] Thermodynamics and analysis of ambient data show that, under conditions of constant temperature and aerosol liquid water, the fraction of nitrate in deliquesced aerosol, $\varepsilon(NO_3^-)$ ($NO_3^-/(NO_3^- + HNO_3(g))$) exhibits an "S-curve" response to aerosol pH (SI Figure S1).[10,22,23] Sufficiently high pH values, usually above 2.5−3,[10,24] ensures that most of the inorganic nitrate condenses onto the aerosol phase,[17,23,25] but a pH below 1 drives all nitrate back into the gas phase. pH in turn is determined by the relative amounts of aerosol water, NH_4^+, SO_4^{2-}, NO_3^- and nonvolatile cations (NVC) from numerous sources,[26] and to a secondary degree organic species and mixing state.[10,27] Source emission patterns, RH, and T are known to vary considerably over space and time, which makes it challenging to unravel the drivers for ambient nitrate, $\varepsilon(NO_3^-)$, and aerosol pH.

Here, we study the impact of source emissions and meteorological parameters (RH, T) on aerosol pH, aerosol nitrate concentrations and $\varepsilon(NO_3^-)$. We first collected data sets of hourly ambient observations of speciated $PM_{2.5}$ during summer in Tianjin, a megacity in northern China, and employed PMF/ME2 (Positive Matrix Factorization using the Multilinear Engine 2, program) source apportionment tools to explore source emission patterns; the ISORROPIA-II thermodynamic model[28] was applied to estimate hourly aerosol pH, and to understand its role on nitrate partitioning and source. We chose summertime because of the more prominent sensitivity of aerosol nitrate to pH than in other seasons due to the favorable conditions of high temperature and RH for semivolatile species in the gas phase. Additionally, summertime meteorological conditions also favor the presence of a metastable aqueous phase, which greatly facilitates the interpretation of data and thus further enhance the robustness of pH estimates. Furthermore, the number of pollutant source categories are fewer in summer than other seasons, which simplifies the attributions of nitrate to its formation pathways. Few field-based studies exist that explore how aerosol pH, RH, T, and source contributions affect nitrate concentrations and $\varepsilon(NO_3^-)$,[10] particularly in China.

MATERIALS AND METHODS

Sampling. Online aerosol and gaseous measurements with 1 h time resolution were conducted in Tianjin, a megacity in northern China, from August 12, 2015 to August 23, 2015. The sampling site was located in a residential area, about 200 m away from a major roadway with dense automobile traffic. Mass concentrations of major water-soluble ions (NH_4^+, Na^+, K^+, Ca^{2+}, Mg^{2+}, SO_4^{2-}, NO_3^-, Cl^-, F^-, NO_2^-) and semivolatile species in the gas phase (HCl, HNO_3, NH_3) were measured by URG9000B samplers (AIM, URG Corporation) with two ICs. Methanesulfonic acid (20 mM) was used for cation analysis and 0.08 mM Na_2CO_3/0.01 mM $NaHCO_3$ was used for anion detection. Both ICs were operated in isocratic elution at a flow rate of 0.5 mL min^{-1}. Concentrations of trace gases (NO_2, SO_2, CO, O_3, NH_3) were measured in hourly temporal resolution by Thermo Fisher Instruments model 42i, model 43i, model 48i, model 49i, model 17i instrument, respectively.

pH Estimation. Aerosol pH is a fundamental property determined by the amount of hydronium ion, H^+, and aerosol water content (eq 1).[17,29] Owing to the lack of an established direct measurement of aerosol pH, thermodynamic analysis of ambient composition data is used to constrain acidity, a method which has been widely used recently.[24,28,30−36] In this study, the ISORROPIA-II inorganic model was employed to estimate gas-particle partitioning, liquid water content and pH for the Na^+-K^+-Ca^{2+}-Mg^{2+}-NH_4^+-SO_4^{2-}-NO_3^--Cl^--H_2O aerosol system.[20,36−39] In total, 387 hourly samples were introduced into ISORROPIA-II to obtain aerosol pH and model concentrations of chemical species (NH_3, NO_3^-, SO_4^{2-}, Cl^-, etc.) in the gas and aerosol phase at thermodynamic equilibrium. Input concentration data included water-soluble ions in $PM_{2.5}$ and semivolatile components in the gas phase (HCl, HNO_3, NH_3) along with RH and T. In this sampling campaign, RH ranged from 47.2% to 79.4% with an average value of 60.1%. The forward (in which known quantities are temperature, relative humidity and the total concentrations of NH_3, H_2SO_4, Na, HCl, HNO_3, and nonvolatile cations Na, K, Ca, Mg) and metastable modes of ISORROPIA-II were selected for the simulations ($CaSO_4$ do precipitate here).[39,40] The detailed information was presented in SI. Aerosol pH was calculated as follows:

$$\mathrm{pH} = -\log_{10}(\gamma_{H^+} m_{H^+}) \quad (1)$$

where m_{H^+} and γ_{H^+} are the molality (mol·kg^{-1} water) and the molality-based activity coefficient of hydrogen ions, respectively.[17,29] γ_{H^+} is assumed to be unity in ISORROPIA-II when single-ion activities for H^+ are required,[28] which introduces only minor uncertainties in pH calculations.[40]

Source Apportionment. Source contribution was calculated with a 1 h time solution by PMF/ME2, a widely used receptor model developed by Paatero.[41,42] Prior information was incorporated into the model in the forms of auxiliary equations, which were included as additional terms $Q_{\partial ux}$ in an enhanced object function Q_{enh}.[43,44] The equation can be written as follows:

$$Q_{enh} = Q_{main} + Q_{\partial ux} \quad (2)$$

DOI: 10.1021/acs.est.8b06524
Environ. Sci. Technol. 2019, 53, 3048−3057

One of the common auxiliary equations is a "pulling equation" that "pulls" f_{pk} (for instance) toward the specific target value ∂_{pk}:

$$Q_{\partial ux} = \frac{(f_{pk} - \partial_{pk})^2}{\sigma_{pk}^{\partial ux^2}} \quad (3)$$

where $\sigma_{pk}^{\partial ux^2}$ is the uncertainty associated with the pulling equation; f_{pk} is the element of factor loading. More description of ME2 was presented in SI. In this study, a data set with 387 rows (number of samples, with 1 h temporal resolution) by 12 columns (number of species) was introduced into PMF/ME2 to apportion pollutant source contributions. The species included NO_3^-, SO_4^{2-}, NH_4^+, Cl^-, F^-, Ca^{2+}, Mg^{2+}, K^+, Na^+, OC, and EC. Source profiles from previous studies[26,45] were used for factor pulling. Ca^{2+} is the marker for dust;[46] EC and OC are the markers of vehicle (exhaust);[47] OC, EC, and Cl^- are the source markers of coal combustion;[48] the markers of secondary sulfate (SS) and secondary nitrate (SN) are ammonium, sulfate, and nitrate.[49]

RESULTS AND DISCUSSION

Water-Soluble Ions, pH, and Sources. Time series of the major water-soluble ions (SNA: SO_4^{2-}, NO_3^-, NH_4^+), and meteorological conditions are presented in Figure 1. The mean

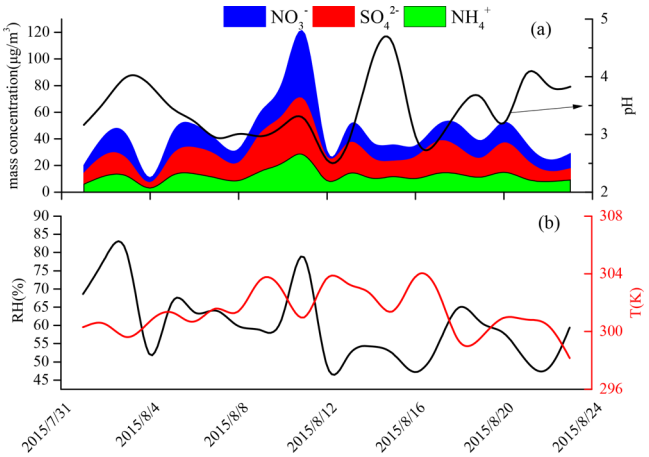

Figure 1. Time series (daily average) of (a) mass concentrations of the major $PM_{2.5}$ species (NO_3^-, SO_4^{2-}, NH_4^+) ($\mu g/m^3$) and aerosol water pH; (b) temperature and RH.

ambient temperature was 301.4K (298.2−303.8 K), and mean RH was 60.1% (47.2−79.4%). The highest concentrations of NO_3^-, SO_4^{2-}, and NH_4^+ were 49.9, 40.9, 27.5 $\mu g\ m^{-3}$, while the lowest were 3.8, 4.0, 3.2 $\mu g\ m^{-3}$, respectively. Concentrations of semivolatile species including NO_3^- and NH_4^+ were negatively correlated with temperature and positively correlated with RH. SO_4^{2-} was positively correlated with T and RH (SI Table S1). Total ammonia (molar concentration of gas-phase ammonia and aerosol ammonium, [TA]) largely exceeded the 2:1 stoichiometric ratio for $(NH_4)_2SO_4$, [TS] (i.e., [TA]-2[TS] > 0).

The calculated aerosol pH ranged from 2.6 to 4.6, with an average of 3.4 ± 0.5 (mean ± standard deviation) (Figure 1); the correlations (r) between measured and modeled concentrations were 0.98 for NO_3^-, 0.98 for NH_4^+ and 0.97 for NH_3 (g); and the regression slopes were 1.02, 1.08, 1.00 for NO_3^-, NH_4^+, and NH_3 (g) (see SI Figure S2, black point) which has been used in the past to support that the pH values are representative.[11,50] Additionally, the root mean squared error (RMSE) and normalized mean bias (NMB) between measured and modeled concentrations were 2.62, 3.63, 4.03 and −0.09, −0.27, 0.16 for NO_3^-, NH_4^+ and NH_3 (g) (see SI Table S2). More detailed information is presented in the SI. In our data, the agreement between estimated and observed gas-phase NH_3 values does not in itself ensure that the pH values are well-constrained—because most of the total ammonia resides in the gas phase, and hence its vapor pressure is insensitive to pH errors.[25] Concentrations of inorganic species in the aerosol and gas-phase are reproduced well by the thermodynamic calculations, including NH_4^+, suggesting that the partitioning fractions of the semivolatile inorganics NH_3/NH_4^+ and HNO_3/NO_3^- are well captured (SI Figure S2). Additionally, sensitivity tests were also performed. One set of tests involved excluding NVCs (all NVC concentrations were set to 0, and using the observed NH_4^+) for calculating pH (identified as "pH*"), to show the importance of using NVCs in ISORROPIA-II for the observed conditions. In SI Figure S2, regression slopes of measured vs predicted values of NH_4^+, NO_3^-, and NH_3 (g) were from 1.00 to 1.13 and R^2s were from 0.97 to 0.99, suggesting that ISORROPIA II captured the partitioning of nitrate and ammonium and that, in this case, the presence of NVCs had a limited impact on the modeled partitioning. Besides, fitted regression equations between pH estimated by E-AIM and by ISORROPIA were shown in SI Figure S2(b). The estimated pH were 3.59 (ISORROPIA) and 3.03 (E-AIM), and the correlation (r) of these two models' results was 0.74, indicated that the pH from two models were similar. Given above information, and that for the RH, T values here a single (metastable) aqueous phase is present suggest the summertime pH values calculated are well constrained by the data.

A matrix of 387 rows (number of samples, with 1 h temporal resolution) by 12 columns (number of chemical species) was introduced into ME2. Five factors were resolved by the model and identified by the source markers. Q_{main} was about 2750 (theoretical Q = 387 × 12−5 × (387 + 12) = 2649). The secondary source factors including secondary sulfate (SS) and secondary nitrate (SN) are formed through complex chemical reactions involving gas precursors. SS and SN were characterized by the presence of ammonium, sulfate, and nitrate.[49] In this work, SN extracted by PMF/ME2 include only condensed phase nitrate, but not nitric acid vapor. The dust factor was determined by relatively high Ca^{2+} abundance;[46] the vehicle factor was distinguished by the high weights of carbonaceous species (EC and OC);[47] and the coal factor was characterized by large proportions of OC, EC, and Cl^-.[48] Detailed source profiles were provided in SI Figure S3. In addition, the hourly time series of contributions from different sources/factor were also calculated by ME2 (SI Figure S3), with average contributions ranked as SS (contributed 25.2% to $PM_{2.5}$), SN (contributed 23.0%), dust (contributed 22.7%), coal (contributed 16.5%), and vehicle (contributed 12.6%). The fitted regression of modeled against measured hourly concentrations of $PM_{2.5}$ are shown in SI Figure S3(d). The regression slope (0.89) and R^2 (0.89) indicate that the performance of source apportionment is satisfactory.

Diurnal Variations of NO_3^-, Sources, and pH. The observed diurnal variations of NO_3^- and pH are presented in

DOI: 10.1021/acs.est.8b06524
Environ. Sci. Technol. 2019, 53, 3048−3057

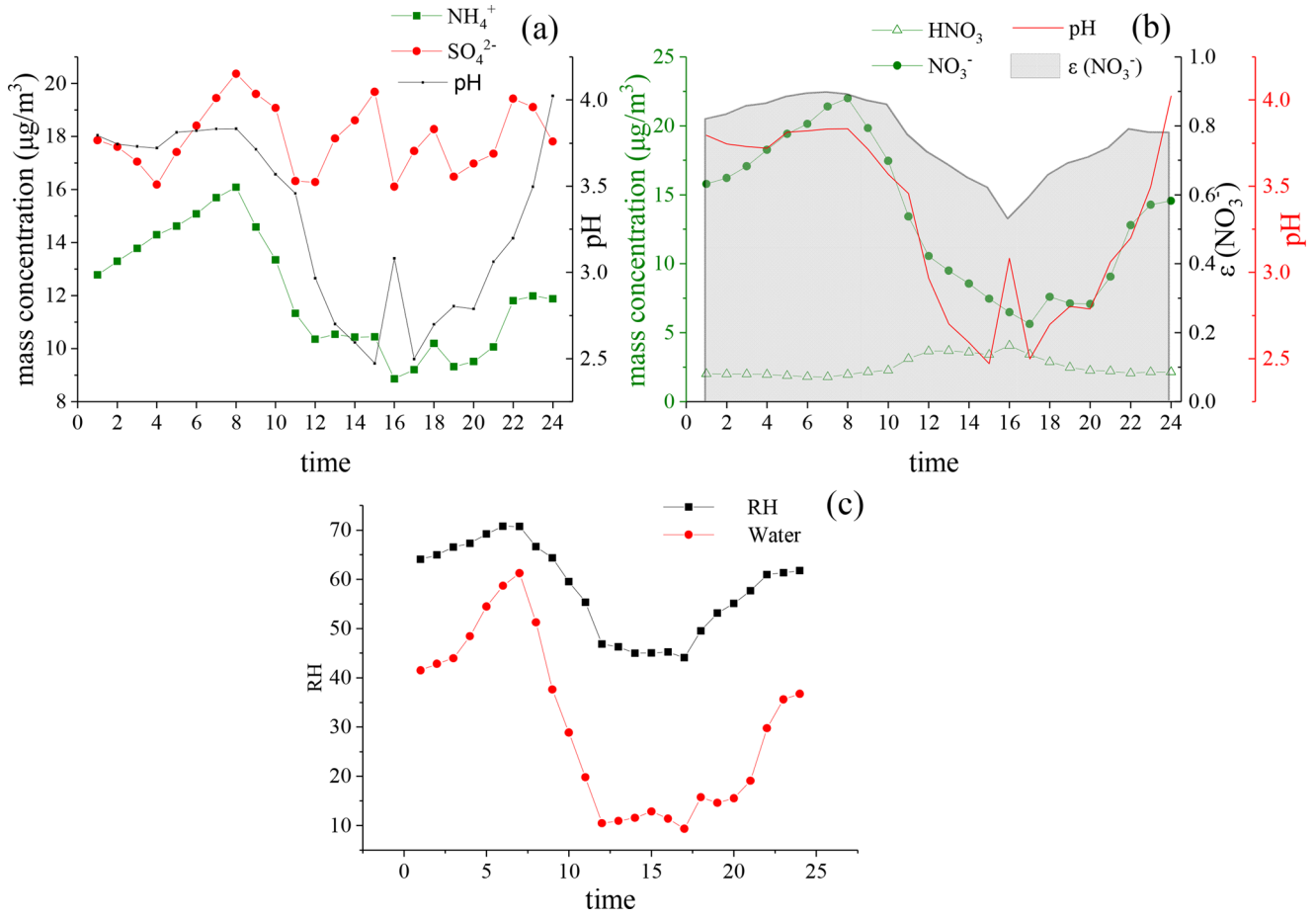

Figure 2. Diurnal patterns of pH, SNA (sulfate, nitrate, ammonium) and HNO_3 concentrations, $\varepsilon(NO_3^-)$ ($NO_3^-/(HNO_3+ NO_3^-)$), water content and RH. $\varepsilon(NO_3^-)$ was calculated using measured HNO_3 ($\mu g/m^3$) and NO_3^- concentrations ($\mu g/m^3$). (a) pH, SO_4^{2-} and NH_4^+ concentrations ($\mu g/m^3$); (b) HNO_3 and NO_3^- concentrations ($\mu g/m^3$), $\varepsilon(NO_3^-)$. Note that SO_4^{2-}, NO_3^-, NH_4^+, NO_3^-, and HNO_3 were all measured concentrations. (c) RH (%) and water content ($\mu g/m^3$, estimated by ISORROPIA II).

Figure 2. To better explore the underlying causes of such variation, we compared the diurnal variations of NO_3^- with those for pH, sources, and other ions (Figure 2). The temporal patterns of NO_3^- exhibited more similarities with pH compared to SO_4^{2-} and NH_4^+. It was partially because low pH can lead to the loss of semivolatile NO_3^-, while high pH can enhance nitrate partitioning into particle phase.[17] Higher SO_4^{2-} fraction in the aerosol, which is also associated with [TS] in the region, tends to decrease pH.[26]

Figure. 2b shows that aerosol pH, NO_3^-, HNO_3 (g) concentrations and $\varepsilon(NO_3^-)$ (calculated as $[NO_3^-]/([HNO_3]+[NO_3^-])$, with $[HNO_3]$ and $[NO_3^-]$ being the mole concentration of gas-phase HNO_3 and aerosol NO_3, respectively (in mole m^{-3}) all have distinct diurnal variations. Aerosol pH was relatively lower during daytime, and higher during nighttime (Figure 2a). HNO_3 (g) concentration ($\mu g\ m^{-3}$) was higher in daytime than nighttime, while NO_3^- concentration ($\mu g\ m^{-3}$) and $\varepsilon(NO_3^-)$ were higher during nighttime than daytime. Such diurnal patterns of HNO_3 (g) can be explained as follows. O_3 concentration and atmospheric temperature were higher during daytime (SI Figure S4) and the diurnal patterns of HNO_3 (g) concentration was opposite to that of NO_x ($NO+NO_2$, reactive precursors of nitrate, SI Figure S5), suggesting that high gaseous HNO_3 during daytime was photochemically driven.[51,52] The high nighttime RH and lower T caused nocturnal NO_3^- to be much higher than daytime (SI Figure S4), because of the nitrate equilibrium constant and aerosol liquid water increases so that equilibrium is shifted to particle phase. Compared with the aerosol pH led by $(NH_4)_2SO_4$, the formation of deliquesced NH_4NO_3 in the aerosol phase tends to increase pH, which in turn favors even more condensation of nitrate and associated ammonium from the gas phase.[10,11] Higher RH in the nighttime than in daytime also promotes higher water content in the aerosol, which drives much of the diurnal variability in aerosol pH.[24,53] Additionally, $\varepsilon(NO_3^-)$ reflects the particle-gas partitioning of nitrate, and it was higher during nighttime and lower during daytime (Figure 2b). The diurnal variation of $\varepsilon(NO_3^-)$ suggested that most of the nitrate was in particle phase, especially during morning and nighttime. Most of the nitrate volatilizes during the day, closely following the trends of T, RH and aerosol pH. In this study, the mean $\varepsilon(NO_3^-)$ was 76.7%, which is lower than that of Song et al. (99.6%, Beijing, China)[40] and higher than that of Guo et al. (45.67%, Pasadena, CA).[25] This result was likely because the sampling campaign of this study was conducted in August (versus winter for Song et al.), and the mean estimated pH in this study was 3.4 vs 4.2 in Song et al.[40] Higher temperature and more acidic environment are expected to enhance nitrate volatilization and its partitioning to gas phase, leading to lower $\varepsilon(NO_3^-)$ in this study.[10,11,17,20]

Emissions from different factors can directly influence aerosol pH.[26] SI Figure S6 shows diurnal variations of factor

DOI: 10.1021/acs.est.8b06524
Environ. Sci. Technol. 2019, 53, 3048−3057

contributions and pH. SS is negatively correlated with pH (especially during daytime) (SI Figure S6c), as sulfuric acid is a strong acid with a very low vapor pressure, thus increased temperatures and lowered RH are expected to lead to reduced aerosol water, consequently concentrating acid. This in turn leads to a persistently acidic aerosol[11,15] which becomes increasingly acidic when concentrations of other aerosol components decrease while the relative proportion of sulfate increases.[15,26] Unlike SS, the correlations between SN contributions and pH were found to be positive (SI Figure S6c) because the pH of pure deliquesced ammonium nitrate (and other nitrate salts with NVCs) is much higher than the pH associated with an aerosol dominated by SS.[25]

SI Figure S6 also presented diurnal variations of contributions from other sources/factors, and pH. Aerosol pH starts decreasing at 7:00 am, and reaches a minimum at about 2:00 pm, a pattern similar to those for dust and coal contributions, but different from vehicle contribution. The heating and expansion of the boundary layer generally leads to the diurnal cycle of RH, that generates a corresponding diurnal cycle in aerosol liquid water. These temporal changes induce a pH diurnal cycle,[17,24,53] which together with the diurnal temperature cycle, generates the diurnal cycle of nitrate partitioning as seen in the data seen here (Figure 2b). However, cations that originate from dust and coal combustion (NH_3/NH_4^+, Ca^{2+}, etc.)[54] can readily increase aerosol pH,[26] so a part of the diurnal pH cycle may be driven by emissions—especially from NVCs (SI Figure S6e). Coal combustion and vehicular traffic also contribute acidic precursors (SO_2, NO_x) which modulate acidity as described above in terms of contributing SS and SN.

Impacts of Aerosol pH on Secondary Nitrate Formation under Different Sources Contributions. When SN contribution (calculated from ME2) is plotted against pH, an interesting "triangle" relationship can be observed (Figure 3); four subregions (identified as A to D) are identified, based on time period, meteorological regime, and source/factor contributions (Figures 3 and 4, and SI Figure S7).

Region A contains relatively few points, mostly observed at night, and is characterized by high $PM_{2.5}$, SNA concentrations and moderate aerosol pH (~ 3.2). Samples in Region B were mostly collected between 0:00−8:00, and were characterized by moderate RH, NO_3^-, NO_2, as well as low SO_4^{2-}, O_3, and temperature. Hence, SN in this region were associated with liquid-phase reactions. It should be noted that aerosol pH in Region B was higher than in other regions (Figure 3) because of its higher liquid water content (SI Figure S8 and S9). Samples in regions B have considerable dust contributions and low contributions from SS (Figure 4), which further increases pH. Also, from Figure 4, as aerosol pH increases, the contributions of SN decreases in Region B (Figure 3), owing to the reductions in total nitrate—which in turn is linked to reductions in NO_x emissions. SS concentrations were relatively lower in region B (Figure 4), which could help promoting aerosol pH increase, as the importance of NVC tends to promote pH to higher values. The large amounts of NH_3 present, which tends to maintain pH high enough to readily promote NO_3 condensation, implies that reductions in SS also decreases SN, because reductions in aerosol liquid water associated with SS loss promotes volatilization of nitrate back to the gas-phase.

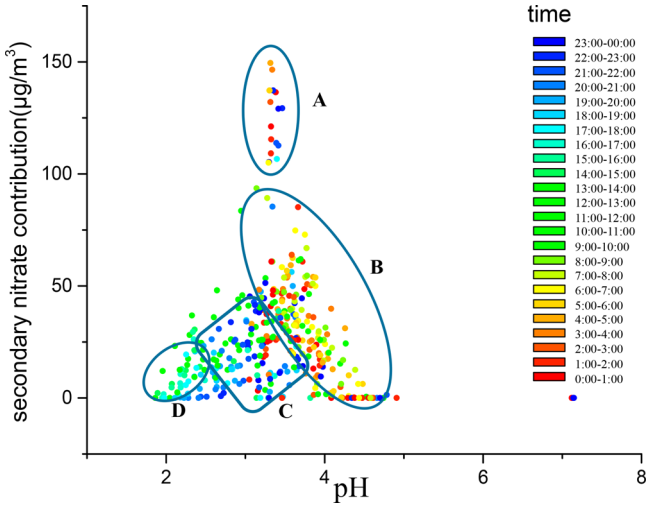

Figure 3. Relationships between aerosol pH and secondary nitrate (SN) contribution. Samples in A−D were collected from different time periods, and were characterized with different meteorological conditions. Detailed information related to meteorological conditions are provided in sI Figure S7.

Samples in Region C were collected between 13:00−00:00, and mostly between 19:00−00:00. Temperature, O_3, and RH were all at moderate levels in this region (SI Figure S7), suggesting that secondary nitrate in Region C was likely formed through both liquid- and gas-phase and photochemical reactions. Samples in Region D were mostly collected between 9:00−17:00, and were characterized by high O_3, temperature (306.0 K), and SO_4^{2-} concentrations, in conjunction with low aerosol pH, NO_3^- concentration, $\varepsilon(NO_3^-)$, and RH (42.1%) (SI Figure S7). The secondary nitrate in this region was likely formed through photochemical reactions. In Region D, T was relatively higher and RH was relatively lower, which would drive nitrate into its gas phase and decrease the nitrate concentrations in particle phase. The aerosols in this region were very acidic (pH from 2 to 2.5) as a result of high liquid H^+ concentration and low water content in the same time period (SI Figures S8 and S9). Also, dust contributed poorly in this region, and thus had little influence on elevating aerosol pH.

Nitrate Partitioning "S-Curve" In Actual Atmospheric Environment. For a NO_3^-- HNO_3 (g) system, under a given constant T and RH, an ideal S-curve relationship between particle-gas partitioning of semivolatile species and aerosol pH (see SI Figure S1) would be found,[12] which can be applied to estimate aerosol pH and aqueous fractions of semivolatile species.[11,15] There are three regions in SI Figure S1. Region (1) and (3) are pH-insensitive bands, where the $\varepsilon(NO_3^-)$ changes slightly with respect to pH change. Region (2) is a pH-sensitive band, where the $\varepsilon(NO_3^-)$ changes drastically with pH. For the ambient data set, the pH-$\varepsilon(NO_3^-)$ curve might be less obvious because T, liquid water content, and ionic strength (activity coefficients) do not remain constant. Here, we plotted $\varepsilon(NO_3^-)$ (calculated from the measured mole concentration of NO_3^- and HNO_3 (g)) ratio against aerosol pH (SI Figure S10). At first glance, no obvious S-curve between $\varepsilon(NO_3^-)$ and pH can be observed. However, after conditional sampling of the data (i.e., when SS contributions are relatively higher, i.e., greater than 25 ug m^{-3}; SI Figure S10(b)), the ambient

DOI: 10.1021/acs.est.8b06524
Environ. Sci. Technol. 2019, 53, 3048−3057

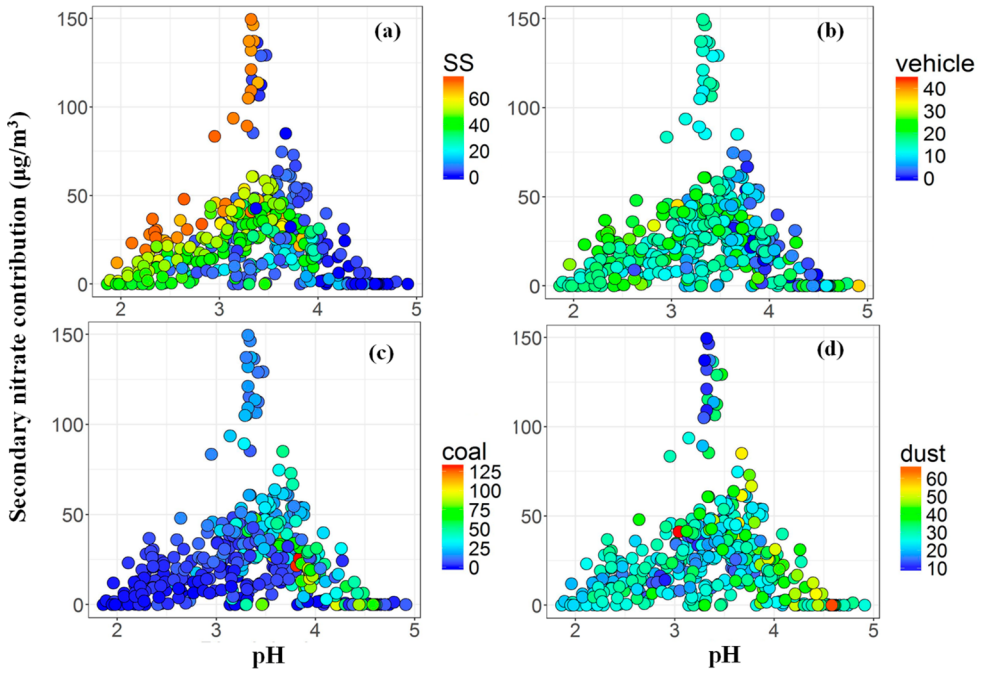

Figure 4. Secondary nitrate contribution (SN) as a function of pH. Circles were color-coded by sources contributions: (a) Secondary sulfate contribution ($\mu g/m^3$), (b) vehicle contribution ($\mu g/m^3$), (c) coal combustion ($\mu g/m^3$), (d) dust contribution ($\mu g/m^3$).

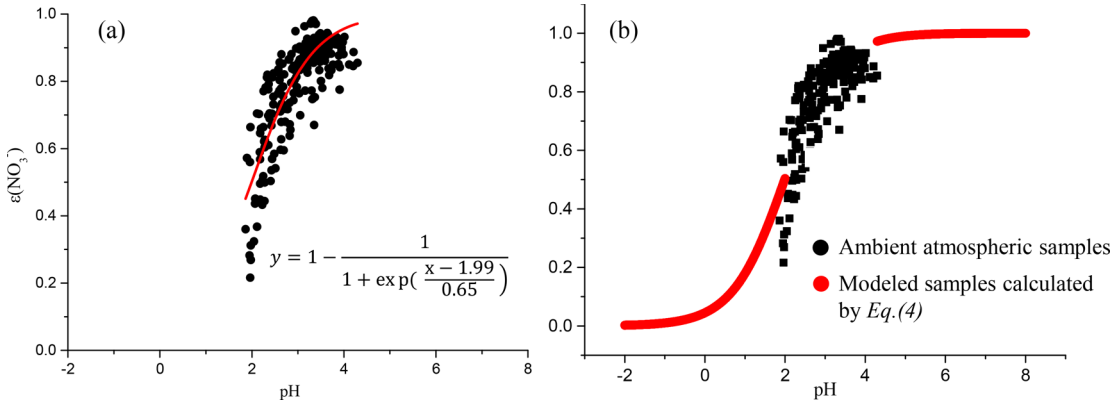

Figure 5. S curve constructed by fitting $\varepsilon(NO_3^-)$ as a function of pH using the Boltzmann equation for summer samples (R^2 = 0.70). Black points are actual atmospheric samples with higher SS contribution (higher than 10 $\mu g\ m^{-3}$); red points are calculated by the Boltzmann equation. $\varepsilon(NO_3^-)$ was calculated using measured NO_3^- concentration in particle phase and measured HNO_3 (g) concentration in gas phase.

samples do captured the pH-$\varepsilon(NO_3^-)$ sensitive band of the S-curve (SI Figure S1).

To empirically describe the relationships between $\varepsilon(NO_3^-)$ ratio and pH, a Boltzmann equation was applied to fit the curve of pH-$\varepsilon(NO_3^-)$. The Boltzmann equation can be used to fit a sigmoid shaped curve and has performed well in the previous works.[55,56]

$$\varepsilon(NO_3^-) = 1 - \frac{1}{1 + e^{(pH-1.99)/0.65}} \quad (4)$$

Origin 8.5 software was employed to perform the curve fitting (χ^2 was 0.007 and R^2 was 0.70) and the result was shown in Figure 5. The fitted curve in Figure 5a is only a portion (sensitive region) of the S-curve, as the range in ambient aerosol pH covers only a fraction of the pH range as encompassed by the entire S-curve (SI Figure S1). eq 4 was extrapolated to outside of the conditions as found in this study, specifically from 0 to 2 and 4−8. Values of the simulated $\varepsilon(NO_3^-)$ ratios (red points in Figure 5b) were also calculated accordingly using (eq 4). Results of the extrapolation are provided in Figure 5b, where the extrapolated data are shown as red points and the actual ambient sample data are shown as black points. The results show that the collected ambient samples (black points) were in the pH-$\varepsilon(NO_3^-)$ sensitive region, indicating that a small change of aerosol pH can have a considerable impact on $\varepsilon(NO_3^-)$ (Figure 5b), which reaches maximum at $\varepsilon(NO_3^-) \sim 0.5$. Nonetheless, there are still a few black points that deviate from the fitted sigmoid curve, possibly due to uncertainties involved in curve fitting and analytical solution. The above statistical analysis shows that an S-curve can be found for the ambient data set in summer.

The existence of an S-curve can also be found in thermodynamic estimations. As shown in eq 5- eq 6:[12]

$$\varepsilon(NO_3^-) = \frac{10^{-6} H_A RTL}{1 + 10^{-6} H_A RTL} \quad (5)$$

DOI: 10.1021/acs.est.8b06524
Environ. Sci. Technol. 2019, 53, 3048−3057

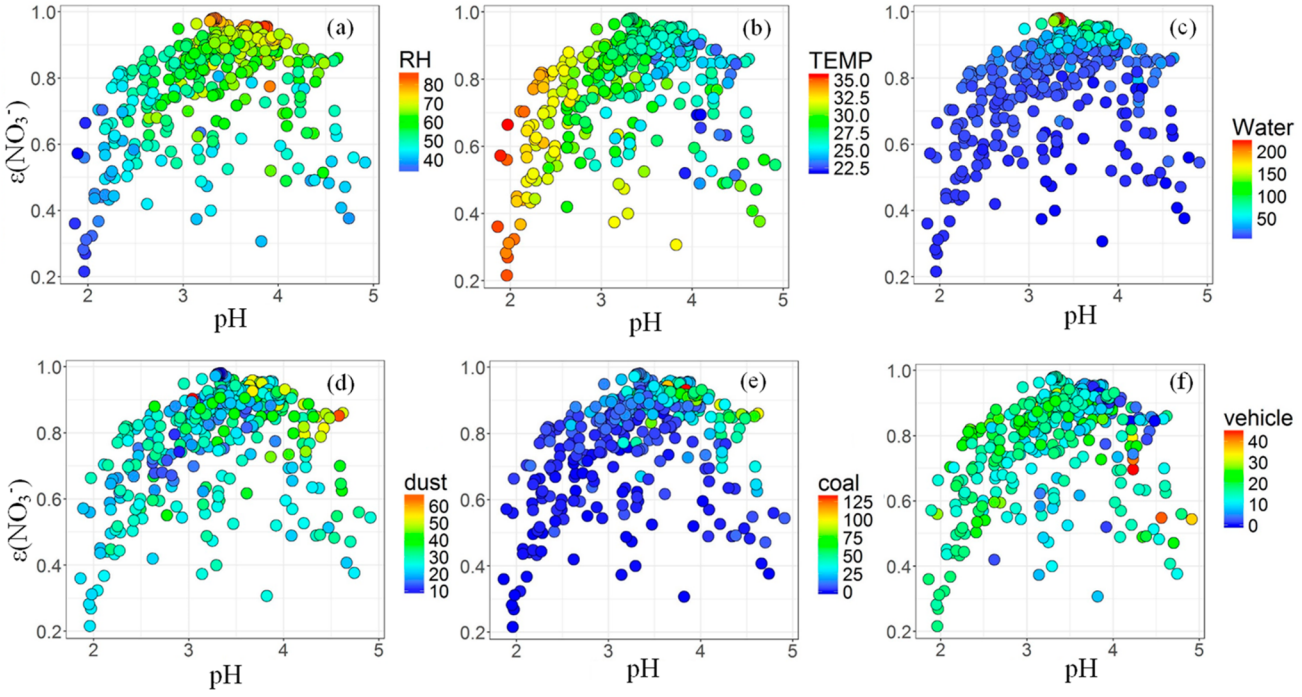

Figure 6. $\varepsilon(NO_3^-)$ as a function of pH under different conditions (a) RH (%); (b) temperature (T, °C); (c) Water content ($\mu g/m^3$); (d) dust contribution ($\mu g/m^3$); (e) coal contribution ($\mu g/m^3$); and (f) vehicle contribution ($\mu g/m^3$). $\varepsilon(NO_3^-)$ was calculated using measured NO_3^- concentration in particle phase and measured HNO_3 (g) concentration in gas phase.

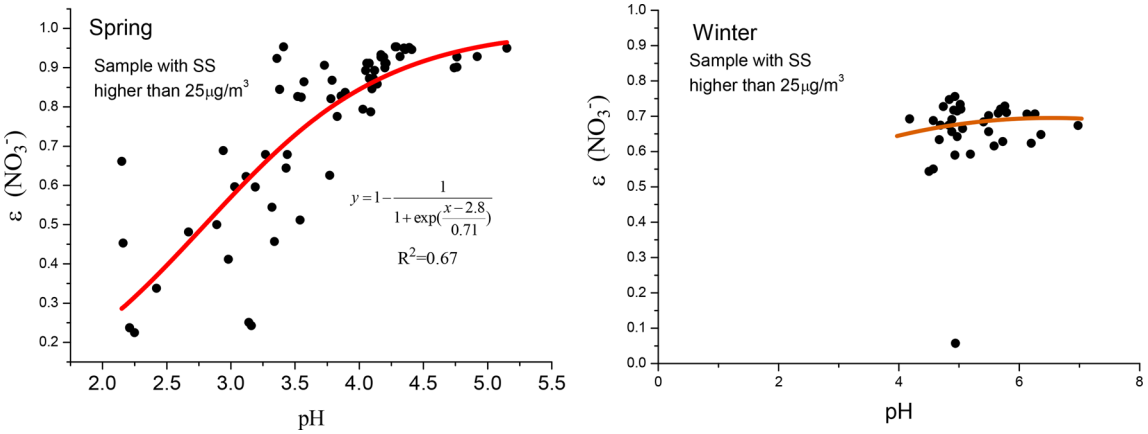

Figure 7. $\varepsilon(NO_3^-)$ vs pH for spring and winter samples when SS was greater than 25 $\mu g\ m^{-3}$.

where H_A is the Henry Law Constant for HNO_3 in M atm^{-1}; R is the ideal-gas constant equal to 0.08205 atm L mol^{-1} K^{-1}; T is the temperature in K; and L is the aerosol liquid water content in g m^{-3} (as estimated by ISORROPIA-II). Given that $H_A \approx \frac{3.2\times10^6}{[H^+]}$[12], and defining 3.2RTL as the index I_{TL}, we obtain

$$\varepsilon(NO_3^-) \approx \frac{I_{TL}}{[H^+] + I_{TL}} \quad (6)$$

Combining the index I_{TL}, pH, and eq 6, we can explain the shape of the pH-$\varepsilon(NO_3^-)$ relationship and help identifying the sensitive band of the S-curve. If $[H^+]$ is in the range of 0.0001 to 0.01 (pH from 2 to 4), $\varepsilon(NO_3^-)$ is sensitive to $[H^+]$. In this work, I_{TL} ranges from 0.0001 to 0.0175, with an average of 0.0026, predominantly in the sensitive range. When pH is less than 2, $[H^+]$ is higher than the maximum value of I_{TL} (0.0175), and the effects of varying T and L on $\varepsilon(NO_3^-)$ can be ignored. When pH is great than 3.3 (especially >4), $[H^+]$ is lower than the minimum value of I_{TL} (0.0001), hence the variation of ambient T and L would greatly influence $\varepsilon(NO_3^-)$ (according to Figure 6, the number of scattered points increased when pH > 3.3). Additionally, when pH is between 2 and 3.3, both $[H^+]$ and I_{TL} can impact $\varepsilon(NO_3^-)$. As observed from Figure 6, there are only limited amounts of scattered points between pH 2–3.3.

Figure 6 also shows the relationships between pH and $\varepsilon(NO_3^-)$ under different meteorological conditions, and for different source categories (in $\mu g\ m^{-3}$, as estimated by ME2). The collected samples in the pH-$\varepsilon(NO_3^-)$ sensitive band were characterized by high SS contribution, moderate vehicle and dust contributions, and low coal contribution. As shown in our previous work, SS dominates in low pH (2–3).[26] Moderate dust contribution would provide nonvolatile cations to

DOI: 10.1021/acs.est.8b06524
Environ. Sci. Technol. 2019, 53, 3048−3057

associate with sulfate and elevate pH. Additionally, moderate vehicle contribution can provide NH_3 and NO_x precursors for nitrate aerosol. The low coal contribution suggests relatively low emissions from coal combustion, thus making the S curve more prominent. We also performed sensitivity tests and found that if the concentrations of sulfate decreases, the shape of $\varepsilon(NO_3^-)$ can be "distorted" because aerosol liquid water is appreciably changed as nitrate condenses and evaporates (SI Figure S11), something that does not occur when SS dominates the liquid water uptake.

Figure 12 shows the relationship between $\varepsilon(NO_3^-)$-pH in other seasons (spring: 2015.4.30−2015.5.30 and winter: 2015.1.4−2015.2.10). Similarly, parts of the S-curves were observed in spring and winter data sets that have higher SS contributions (Figure 7). For spring, the pH-sensitive band was fit to a sigmoid curve: $\varepsilon(NO_3^-) = 1 - \frac{1}{1+e^{(pH-2.8)/0.71}}$, ($R^2$ = 0.67). For winter, the pH-insensitive band (right band, Figure 7) was found, likely due to the considerable variability in aerosol liquid water, temperature, and emissions patterns over the time period examined. I_{TL} ranged from 0.0000 to 0.0094, with an average of 0.00067 for spring samples. So, the range of pH for sensitive band of the S-curve should be from 2 to 4, which can be confirmed by Figure 7 (left side, spring). Additionally, I_{TL} ranged from 0.0000 to 0.012, with an average of 0.0013 for winter samples, suggesting that the range of pH for sensitive band should from 1 to 4. In Guo et al. (2017), the S-curves were found in the range of pH from −1 to 3 in winter. But in this work, pHs typically were higher than 3 in winter (see SI Figure S12), so nitrate partitioning tends to reside in the upper "plateau" of the S-curve, which are modulated by variations in T and L. Similar as in the summer, TN (NO_3^-+HNO_3 (g)) vs pH for winter and spring seasons yield "triangles," indicating that similar emissions and chemical domains are responsible for the behavior. A detailed discussion can be found in the SI.

IMPLICATIONS

The use of highly time-resolved (hourly) observations of aerosol compositions over multiple seasons allowed more detailed examination of the aerosol thermodynamics in different seasons, and the relationships between aerosol composition, sources, pH, and meteorological factors. In this study, aerosol pH ranges from 2.6 to 4.6, with an average pH of 3.4 ± 0.5. The gas-particle partitioning of the observed semivolatile inorganic species (ammonia-ammonium and nitric acid-nitrate) are consistent with the thermodynamics of the ammonia-sulfate-nitrate-NVC system. An interesting "triangle" relationship was found between the SN contribution and pH. This was found to primarily be linked to the emissions of nitrate precursors (NO_x and NH_3) and physicochemical processes leading to SN formation. A triangular shape relationship between SN and pH is found. In more polluted environments, in conditions favorable for SN formation (i.e., lower temperatures, higher RH) the pH is pushed toward the value of pure ammonium nitrate's; as SS increases, pH decreases (left side of triangle), while a higher fraction of NVCs raises pH because TN and SS decrease (right side of triangle) when the air masses are cleaner.

The use of hourly samples further support that the "S-curve" nitrate-nitric acid gas and ammonium-ammonia gas partitioning relationships, particularly when SS levels are higher, leading to greater aerosol water levels. The index (I_{TL}) developed in this work, can help determining when nitrate partitioning is in the pH-sensitive region. This region is also where ammonia and NO_x emissions control strategies are both efficient in reducing the nitrate aerosol load, though sulfate reductions will be less efficient. But at very high or low I_{TL}'s, this substitution is less important. Given that the I_{TL}'s vary throughout the day, the use of hourly observations can be important as 24 h samples can mis-identifying times when controls are effective.

ASSOCIATED CONTENT

Supporting Information

The Supporting Information is available free of charge on the ACS Publications website at DOI: 10.1021/acs.est.8b06524.

Figures S1−S13 (PDF)

AUTHOR INFORMATION

Corresponding Author

*E-mail: nksgl@nankai.edu.cn.

ORCID

Shaojie Song: 0000-0001-6395-7422

Haofei Yu: 0000-0002-7930-8934

Guoliang Shi: 0000-0001-5872-0236

Notes

The authors declare no competing financial interest.

ACKNOWLEDGMENTS

This study was supported by the National Natural Science Foundation of China (41775149), National Key Research and Development Program of China (2016YFC0208500, 2016YFC0208505), Special Scientific Research Funds for Environment Protection Commonweal Section (Nos. 201509020), the Tianjin Research Program of Application Foundation and Advanced Technology (14JCQNJC0810), Tianjin Natural Science Foundation (17JCYBJC23000, 16JCQNJC08700), and the Blue Sky Foundation, Fundamental Research Funds for the Central Universities. This publication was developed under Assistance Agreement No. EPA834799 awarded by the U.S. Environmental Protection Agency to Emory University and Georgia Institute of Technology. It has not been formally reviewed by EPA. The views expressed in this document are solely those of the authors and do not necessarily reflect those of the Agency. EPA does not endorse any products or commercial services mentioned in this publication. We also acknowledge support from the project PyroTRACH (ERC-2016-COG) funded from H2020-EU.1.1. - Excellent Science - European Research Council (ERC), project ID 726165. We also thank Ms. G. Pavur for her help in preparing the manuscript.

REFERENCES

(1) Wu, C.; Wang, G. H.; Wang, J. Y.; Li, J. J.; Ren, Y. Q.; Zhang, L.; Cao, C.; Li, J.; Ge, S. S.; Xie, Y. N.; Wang, X. P.; Xue, G. Y. Chemical characteristics of haze particles in Xi'an during Chinese Spring Festival: Impact of fireworks burning. *J. Environ. Sci.* **2018**, *71*, 179−187.

(2) Yao, X.; Chan, C. K.; Fang, M.; Cadle, S.; Chan, T.; Mulawa, P.; He, K.; Ye, B. The water-soluble ionic composition of PM2.5 in Shanghai and Beijing, China. *Atmos. Environ.* **2002**, *36*, 4223−4234.

(3) Qiao, T.; Zhao, M.; Xiu, G.; Yu, J. Seasonal variations of water soluble composition (WSOC, Hulis and WSIIs) in PM1 and its implications on haze pollution in urban Shanghai, China. *Atmos. Environ.* **2015**, *123*, 306−314.

DOI: 10.1021/acs.est.8b06524
Environ. Sci. Technol. 2019, 53, 3048−3057

(4) Hua, Y.; Cheng, Z.; Wang, S. X.; Jiang, J. K.; Chen, D. R.; Cai, S. Y.; Fu, X.; Fu, Q. Y.; Chen, C. H.; Xu, B. Y.; Yu, J. Q. Characteristics and source apportionment of PM2.5 during a fall heavy haze episode in the Yangtze River Delta of China. *Atmos. Environ.* **2015**, *123*, 380−391.
(5) Tian, Y. Z.; Liu, J. Y.; Han, S. Q.; Shi, X. R.; Shi, G. L.; Xu, H.; Yu, H. F.; Zhang, Y. F.; Feng, Y. C.; Russell, A. G. Spatial, seasonal and diurnal patterns in physicochemical characteristics and sources of PM2.5 in both inland and coastal regions within a megacity in China. *J. Hazard. Mater.* **2018**, *342*, 139−149.
(6) Gao, J.; Peng, X.; Chen, G.; Xu, J.; Shi, G. L.; Zhang, Y. F.; Feng, Y. C. Insights into the chemical characterization and sources of PM2.5 in Beijing at a 1-h time resolution. *Sci. Total Environ.* **2016**, *532*, 162−171.
(7) Wang, X. F.; Zhang, Y. P.; Chen, H.; Yang, X.; Chen, J. M. Particulate nitrate formation in a highly polluted urban area: a case study by single-particle mass spectrometry in Shanghai. *Environ. Sci. Technol.* **2009**, *43*, 3061−3066.
(8) Fu, X. X.; Guo, H.; Wang, X. M.; Ding, X.; He, Q. F.; Liu, T. Y.; Zhang, Z. PM2.5 acidity at a background site in the Pearl River Delta region in fall-winter of 2007−2012. *J. Hazard. Mater.* **2015**, *286*, 484−492.
(9) Xue, J.; Yuan, Z. B.; Lau, A. K. H.; Yu, J. Z. Insights into factors affecting nitrate in PM2.5 in a polluted high NO_x environment through hourly observations and size distribution measurements. *J. Geophys. Res. Atmos.* **2014**, *119* (8), 4888−4902.
(10) Guo, H. Y.; Otjes, R.; Schlag, P.; Kiendler-Scharr, A.; Nenes, A.; Weber, R. J. Effectiveness of ammonia reduction on control of fine particle nitrate. *Atmos. Chem. Phys.* **2018**, *18*, 12241−12256.
(11) Guo, H. Y.; Weber, R. J.; Nenes, A. High levels of ammonia do not raise fine particle pH sufficiently to yield nitrogen oxide-dominated sulfate production. *Sci. Rep.* **2017a**, *7*, 12109.
(12) Seinfeld, J. H.; Pandis, S. N. *Atmospheric Chemistry and Physics: From Air Pollution to Climate Change*, 3rd ed.; John Wiley & Sons: Hoboken, NJ, 2016.
(13) Cheng, Y.; Zheng, G.; Wei, C.; Mu, Q.; Zheng, B.; Wang, Z.; Gao, M.; Zhang, Q.; He, K.; Carmichael, G.; Pöschl, U.; Su, H. Reactive nitrogen chemistry in aerosol water as a source of sulfate during haze events in China. *Sci. Adv.* **2016**, *2*, No. e1601530.
(14) Xu, L.; Guo, H.; Boyd, C. M.; Klein, M.; Bougiatioti, A.; Cerully, K. M.; Hite, J. R.; Isaacman-VanWertz, G.; Kreisberg, N. M.; Knote, C.; Olson, K.; Koss, A.; Goldstein, A. H.; Hering, S. V.; de Gouw, J.; Baumann, K.; Lee, S.-H.; Nenes, A.; Weber, R. J.; Ng, N. L. Effects of anthropogenic emissions on aerosol formation from isoprene and monoterpenes in the southeastern United States. *Proc. Natl. Acad. Sci. U. S. A.* **2015**, *112*, 37−42.
(15) Weber, R. J.; Guo, H.; Russell, A. G.; Nenes, A. High aerosol acidity despite declining atmospheric sulfate concentrations over the past 15 years. *Nat. Geosci.* **2016**, *9*, 282−285.
(16) Keene, W. C.; Pszenny, A. A. P.; Maben, J. R.; Stevenson, E.; Wall, A. Closure evaluation of size-resolved aerosol pH in the New England coastal atmosphere during summer. *J. Geophys. Res. Atmos.* **2004**, *109*, D23307.
(17) Guo, H. Y.; Weber, R. J.; Nenes, A. High levels of ammonia do not raise fine particle pH sufficiently to yield nitrogen oxide-dominated sulfate production. *Sci. Rep.* **2017a**, *7*, 12109.
(18) Longo, A. F.; Feng, Y.; Lai, B.; Landing, W. M.; Shelley, R. U.; Nenes, A.; Mihalopoulos, N.; Violaki, K.; Ingall, E. D. Influence of Atmospheric Processes on the Solubility and Composition of Iron in Saharan Dust. *Environ. Sci. Technol.* **2016**, *50*, 6912−6920.
(19) Nenes, A.; Krom, M. D.; Mihalopoulos, N.; Van Cappellen, P.; Shi, Z.; Bougiatioti, A.; Zarmpas, P.; Herut, B. Atmospheric acidification of mineral aerosols: A source of bioavailable phosphorus for the oceans. *Atmos. Chem. Phys.* **2011**, *11*, 6265−6272.
(20) Meskhidze, N.; Chameides, W.; Nenes, A.; Chen, G. Iron Mobilization in Mineral Dust: Can Anthropogenic SO2 Emissions Affect Ocean Productivity? *Geophys. Res. Lett.* **2003**, *30* (21), 2085.
(21) Fang, T.; Guo, H.; Zeng, L.; Verma, V.; Nenes, A.; Weber, R. J. Highly acidic ambient particles, soluble metals and oxidative potential: A link between sulfate and aerosol toxicity. *Environ. Sci. Technol.* **2017**, *51* (5), 2611−2620.
(22) Nah, T.; Guo, H. Y.; Sullivan, A. P.; Chen, Y. L.; Tanner, D. J.; Nenes, A.; Russell, A. G.; Ng, N. L.; Huey, L. G.; Weber, R. J. Characterization of aerosol composition, aerosol acidity and organic acid partitioning at an agriculture-intensive rural southeastern U. S. Site. *Atmos. Chem. Phys.* **2018**, *18*, 11471−11491.
(23) Vasilakos, P.; Russell, A. G.; Weber, R. J.; Nenes, A. Understanding nitrate formation in a world with less sulfate. *Atmos. Chem. Phys.* **2018**, *18*, 12765−12775.
(24) Bougiatioti, A.; Nikolaou, P.; Stavroulas, I.; Kouvarakis, G.; Weber, R.; Nenes, A.; Kanakidou, M.; Mihalopoulos, N. Particle water and pH in the eastern Mediterranean: source variability and implications for nutrient availability. *Atmos. Chem. Phys.* **2016**, *16*, 4579−4591.
(25) Guo, H. Y.; Liu, J.; Froyd, K. D.; Roberts, J. M.; Veres, P. R.; Hayes, P. L.; Jimenez, J. L.; Nenes, A.; Weber, R. J. Fine particle pH and gas−particle phase partitioning of inorganic species in Pasadena, California, during the 2010 CalNex campaign. *Atmos. Chem. Phys.* **2017b**, *17*, 5703−5719.
(26) Shi, G. L.; Xu, J.; Peng, X.; Xiao, Z. M.; Chen, K.; Tian, Y. Z.; Guan, X. B.; Feng, Y. C.; Yu, H. F.; Nenes, A.; Russell, A. G. pH of aerosols in a polluted atmosphere: source contributions to highly acidic aerosol. *Environ. Sci. Technol.* **2017**, *51*, 4289−4296.
(27) Pye, H. O. T.; Zuend, A.; Fry, J. L.; Isaacman-VanWertz, G.; Capps, S. L.; Appel, K. W.; Foroutan, H.; Xu, L.; Ng, N. L.; Goldstein, A. H. Coupling of organic and inorganic aerosol systems and the effect on gas-particle partitioning in the southeastern United States. *Atmos. Chem. Phys.* **2018**, *18*, 357−370.
(28) Fountoukis, C.; Nenes, A. ISORROPIA II: a computationally efficient thermodynamic equilibrium model for K+-Ca2+-Mg2+-NH4+-Na+-SO42−-NO3−-Cl−-H2O aerosols. *Atmos. Chem. Phys.* **2007**, *7* (17), 4639−4659.
(29) Battaglia, M. A.; Douglas, S.; Hennigan, C. J. Effect of the urban heat island on aerosol pH. *Environ. Sci. Technol.* **2017**, *51*, 13095−13103.
(30) Clegg, S. L.; Brimblecombe, P.; Wexler, A. S. Thermodynamic model of the system H+-NH4+-SO42−-NO3−-H2O at tropospheric temperatures. *J. Phys. Chem. A* **1998**, *102* (12), 2137−2154.
(31) Guo, H. Y.; Liu, J.; Froyd, K. D.; Roberts, J. M.; Veres, P. R.; Hayes, P. L.; Jimenez, J. L.; Nenes, A.; Weber, R. J. Fine particle pH and gas−particle phase partitioning of inorganic species in Pasadena, California, during the 2010 CalNex campaign. *Atmos. Chem. Phys.* **2017c**, *17*, 5703−5719.
(32) Parworth, C. L.; Young, D. E.; Kim, H.; Zhang, X.; Cappa, C. D.; Collier, S.; Zhang, Q. Wintertime water-soluble aerosol composition and particle water content in Fresno, California. *J. Geophys. Res. Atmos.* **2017**, *122*, 3155−3170.
(33) Murphy, J. G.; Gregoire, P. K.; Tevlin, A. G.; Wentworth, G. R.; Ellis, R. A.; Markovic, M. Z.; VandenBoer, T. C. Observational constraints on particle acidity using measurements and modelling of particles and gases. *Faraday Discuss.* **2017**, *200*, 379−395.
(34) Yao, X.; Ling, T. Y.; Fang, M.; Chan, C. K. Size dependence of in situ pH in submicron atmospheric particles in Hong Kong. *Atmos. Environ.* **2007**, *41*, 382−393.
(35) Zhang, Q.; Jimenez, J. L.; Worsnop, D. R.; Canagaratna, M. A case study of urban particle acidity and its influence on secondary organic aerosol. *Environ. Sci. Technol.* **2007**, *41*, 3213−3219.
(36) Nenes, A.; Pandis, S. N.; Pilinis, C. ISORROPIA: A new thermodynamic equilibrium model for multiphase multicomponent inorganic aerosols. *Aquat. Geochem.* **1998**, *4* (1), 123−152.
(37) Fountoukis, C.; Nenes, A.; Sullivan, A.; Weber, R.; Van Reken, T.; Fischer, M.; Matias, E.; Moya, M.; Farmer, D.; Cohen, R. C. Thermodynamic characterization of Mexico City aerosol during MILAGRO 2006. *Atmos. Chem. Phys.* **2009**, *9* (6), 2141−2156.
(38) Nowak, J. B.; Huey, L. G.; Russell, A. G.; Tian, D.; Neuman, J. A.; Orsini, D.; Sjostedt, S. J.; Sullivan, A. P.; Tanner, D. J.; Weber, R. J.; Nenes, A.; Edgerton, E.; Fehsenfeld, F. C. Analysis of urban gas phase ammonia measurements from the 2002 Atlanta Aerosol

DOI: 10.1021/acs.est.8b06524
Environ. Sci. Technol. 2019, 53, 3048−3057

Nucleation and Real-Time Characterization Experiment (ANARChE). *J. Geophys. Res.* **2006**, *111* (D17), D17308.
(39) Hennigan, C. J.; Izumi, J.; Sullivan, A. P.; Weber, R. J.; Nenes, A. A critical evaluation of proxy methods used to estimate the acidity of atmospheric particles. *Atmos. Chem. Phys.* **2015**, *15* (5), 2775−2790.
(40) Song, S. J.; Gao, M.; Xu, W. Q.; Shao, J. Y.; Shi, G. L.; Wang, S. X.; Wang, Y. X.; Sun, Y. L.; McElroy, M. B. Fine-particle pH for Beijing winter haze as inferred from different thermodynamic equilibrium models. *Atmos. Chem. Phys.* **2018**, *18*, 7423−7438.
(41) Guo, H. Y.; Liu, J.; Froyd, K. D.; Roberts, J. M.; Veres, P. R.; Hayes, P. L.; Jimenez, J. L.; Nenes, A.; Weber, R. J. Fine particle pH and gas−particle phase partitioning of inorganic species in Pasadena, California, during the 2010 CalNex campaign. *Atmos. Chem. Phys.* **2017c**, *17*, 5703−5719.
(42) Paatero, P. *End User's Guide to Multilinear Engine Applications*. 2007.
(43) Amato, F.; Pandolfi, M.; Escrig, A.; Querol, X.; Alastuey, A.; Pey, J.; Perez, N.; Hopke, P. K. Quantifying road dust resuspension in urban environment by Multilinear Engine: A comparison with PMF2. *Atmos. Environ.* **2009**, *43*, 2770−278.
(44) Amato, F.; Hopke, P. K. Source apportionment of the ambient PM2.5 across St. Louis using constrained positive matrix factorization. *Atmos. Environ.* **2012**, *46*, 329−337.
(45) Shi, G. L.; Liu, J. Y.; Wang, H. T.; Tian, Y. Z.; Wen, J.; Shi, X. R.; Feng, Y. C.; Ivey, C. E.; Russell, A. G. Source apportionment for fine particulate matter in a Chinese city using an improved gas-constrained method and comparison with multiple receptor models. *Environ. Pollut.* **2018**, *233*, 1058−1067.
(46) Pant, P.; Harrison, R. M. Critical review of receptor modelling for particulate matter: a case study of India. *Atmos. Environ.* **2012**, *49*, 1−12.
(47) Tian, Y. Z.; Liu, J. Y.; Han, S. Q.; Shi, X. R.; Shi, G. L.; Xu, H.; Yu, H. F.; Zhang, Y. F.; Feng, Y. C.; Russell, A. G. Spatial, seasonal and diurnal patterns in physicochemical characteristics and sources of $PM_{2.5}$ in both inland and coastal regions within a megacity in China. *J. Hazard. Mater.* **2018**, *342*, 139−149.
(48) Tian, Y. Z.; Shi, G. L.; Han, B.; Wu, J. H.; Zhou, X. Y.; Zhou, L. D.; Zhang, P.; Feng, Y. C. Using an improved source directional apportionment method to quantify the $PM_{2.5}$ source contributions from various directions in a megacity in China. *Chemosphere* **2015**, *119*, 750−756.
(49) Guo, H. Y.; Liu, J.; Froyd, K. D.; Roberts, J. M.; Veres, P. R.; Hayes, P. L.; Jimenez, J. L.; Nenes, A.; Weber, R. J. Fine particle pH and gas−particle phase partitioning of inorganic species in Pasadena, California, during the 2010 CalNex campaign. *Atmos. Chem. Phys.* **2017c**, *17*, Waked-3346.57035719
(50) Wang, G.; Zhang, R.; Gomez, M. E.; Yang, L.; Levy Zamora, M.; Hu, M.; Lin, Y.; Peng, J.; Guo, S.; Meng, J.; Li, J.; Cheng, C.; Hu, T.; Ren, Y.; Wang, Y.; Gao, J.; Cao, J.; An, Z.; Zhou, W.; Li, G.; Wang, J.; Tian, P.; Marrero-Ortiz, W.; Secrest, J.; Du, Z.; Zheng, J.; Shang, D.; Zeng, L.; Shao, M.; Wang, W.; Huang, Y.; Wang, Y.; Zhu, Y.; Li, Y.; Hu, J.; Pan, B.; Cai, L.; Cheng, Y.; Ji, Y.; Zhang, F.; Rosenfeld, D.; Liss, P. S.; Duce, R. A.; Kolb, C. E.; Molina, M. J. Persistent sulfate formation from London Fog to Chinese haze. *Proc. Natl. Acad. Sci. U. S. A.* **2016**, *113*, 13630−13635.
(51) Eddingsaas, N. C.; VanderVelde, D. G.; Wennberg, P. O. Kinetics and products of the acid-catalyzed ring-opening of atmospherically relevant butyl epoxy alcohols. *J. Phys. Chem. A* **2010**, *114* (31), 8106−8113.
(52) Sandford, R. C.; Exenberger, A.; Worsfold, P. J. Nitrogen cycling in natural waters using in situ, reagentless UV spectrophotometry with simultaneous determination of nitrate and nitrite. *Environ. Sci. Technol.* **2007**, *41* (24), 8420−8425.
(53) Guo, H. Y.; Xu, L.; Bougiatioti, A.; Cerully, K. M.; Capps, S. L.; Hite, J. R., Jr.; Carlton, A. G.; Lee, S.-H.; Bergin, M. H.; Ng, N. L.; Nenes, A.; Weber, R. J. Fine-particle water and pH in the southeastern United States. *Atmos. Chem. Phys.* **2015**, *15*, 5211−5228.
(54) Marmur, A.; Unal, A.; Mulholland, J. A.; Russell, A. G. Optimization-Based source apportionment of PM2.5 incorporating gas-to-particle ratios. *Environ. Sci. Technol.* **2005**, *39*, 3245−3254.
(55) Jamieson, L. E.; Jaworska, A.; Jiang, J.; Baranska, M.; Harrison, D.; Campbell, C. Simultaneous intracellular redox potential and pH measurements in live cells using SERS nanosensors. *Analyst* **2015**, *140* (7), 2330−2335.
(56) Wei, H. R.; Vejerano, E. P.; Leng, W. N.; Huang, Q. S.; Willner, M. R.; Marr, L. C.; Vikesland, P. J. Aerosol microdroplets exhibit a stable pH gradient. *Proc. Natl. Acad. Sci. U. S. A.* **2018**, *115* (28), 7272−7277.

DOI: 10.1021/acs.est.8b06524
Environ. Sci. Technol. 2019, 53, 3048−3057